REAL TIME AM-FM ANALYSIS OF ULTRASOUND VIDEO

Paul Rodriguez V. and M. S. Pattichis

image and video Processing and Communications Lab (ivPCL)
Dept of EECE, The University of New Mexico, Albuquerque, NM 87131-1356

ABSTRACT

In this paper, we present a real-time amplitude-modulation frequency-modulation (AM-FM) analysis system, and apply the system to M-mode ultrasound video. The estimated frequency-modulation (fm) process is shown to capture the cardiac wall deformation, while the amplitude modulation process is shown to follow changes in cardiac wall material. Results from segmenting the septum and left-ventricle walls are also presented.

1. INTRODUCTION

In M-mode ultrasound video, a ray of points is tracked through time, leading to an observation of cardiac wall deformations (M in M-mode stands for motion) [1]. An example video image is shown in Figure 1.

To recognize a suitable AM-FM series for the M-mode ultrasound video image, we consider the row-column coordinate system $y-t$ where y is used for indexing the rows, while the time coordinate t is used for indexing the columns. Along the y-coordinate, the ultrasound video image is "cutting through" cardiac wall boundaries, showing a single line of the 3-D object points. Along the time-coordinate t, it is assumed that the motion of the same 3-D wall points are observed through time. This is illustrated in Figure 1. Clearly, the assumption is violated if there is significant motion in the ultrasound probe acquiring the video.

To track the wall motion, we consider the use of a curvilinear coordinate system that models wall-motion through a frequency modulation process, while variation in the actual wall material is described through an amplitude modulation process. We model M-mode video in terms of an AM-FM series expansion given by [2]

$$f(y,t)=\sum_n C_n a(y,t)\cos\left(n\phi(y,t)\right), \qquad (1)$$

where ϕ denotes the phase function, $\cos\left(n\phi(y,t)\right)$ denotes the FM harmonics, $a(.)$ denotes the amplitude function, and C_n represents the coefficients of the AM-FM harmonics. We also define the instantaneous frequency as $\nabla\phi$, and its magnitude by the vector magnitude $\|\nabla\phi\|$. In what follows, we set $x=t$ to represent images in the familiar $x-y$ coordinate system.

In Section 2, we summarize the main concepts associated with multidimensional AM-FM demodulation, and develop some modifications that allow robust, real-time operation. The results are summarized in Section 3. Concluding remarks are given in Section 4.

2. REAL-TIME AM-FM DEMODULATION

The basic AM-FM demodulation algorithm is summarized in the following steps [3]:

Step 1. Compute "Analytic Image" using 2-d FFT
Step 2. Apply bandpass channel filters
Step 3. Compute AM-FM parameters over each channel
Step 4. At each pixel, reconstruct AM-FM image using the channel that produces the maximum amplitude estimate

Here, we define the AM-FM demodulation problem, as one of having to estimate the amplitude $a(x,y)$, the phase $\phi(x,y)$, and the instantaneous-frequency vector

$$\nabla\phi(x,y)=\left[\partial\phi/\partial x,\partial\phi/\partial y\right]^T,$$

from the original image.

To estimate the AM-FM parameters, we apply a collection of Gabor (bandpass) channel filters $g_1,g_2,...,g_R$ to the image f, obtaining output images $h_1,h_2,...,h_R$ satisfying $h_i=f*g_i$ where $*$ denotes convolution. Let $G_1,G_2,...,G_R$ denote the frequency responses of the Gabor channel filters. We then obtain estimates for the instantaneous frequency and the phase using [2-4]:

$$\nabla\phi_i(x,y)\cong \text{real}\left\{\frac{\nabla h_i(x,y)}{jh_i(x,y)}\right\},$$
$$\phi_i(x,y)\cong \arctan\left\{\frac{\text{imaginary}\{h_i(x,y)\}}{\text{real}\{h_i(x,y)\}}\right\}. \qquad (2)$$

Using the instantaneous frequency estimate $\nabla\phi(x,y)$ and the frequency response of the Gabor channel G_i, we estimate the amplitude over each channel using

$$a_i(x,y)\cong\left|\frac{h_i(x,y)}{G_i\left(\nabla\phi(x,y)\right)}\right|. \qquad (3)$$

In the Dominant Component Analysis (DCA) algorithm, from the estimates for each channel filter, we select the estimates

0-7803-7523-8/02/$17.00 ©2002 IEEE

from the channel with the maximum amplitude estimate: $c_{\max}(x,y) = \underset{i}{\text{argmax}}\ a_i(x,y)$. Hence, the algorithm adaptively selects the channel filter with the maximum response. This approach does not assume spatial continuity, and allows the model to quickly adapt to singularities in the image. The performance of the AM-FM demodulation algorithm in one and two-dimensions has been studied in [2-4]. A discrete-space algorithm is also described in [2,3].

Next, we present a number of modifications to the basic algorithm that allow us to achieve real-time performance. In addition, we discuss how to achieve robustness.

2.1 Real-time implementation

To achieve real-time AM-FM demodulation, we modify the original algorithm using:

- a small number of channel filters

Only two bandpass filters are used for implementing AM-FM demodulation.

- a separable filter design

A separable implementation along the horizontal and vertical directions is possible due to strong modulation in the vertical direction. As shown in [2, 7], it is always possible to consider the phase function to be separable along the directions of the eigenvectors of the instantaneous frequency gradient tensor (IFGT). In this case, the eigenvector in the direction of the largest eigenvalue is in the vertical direction, while the direction of minimal modulation is along the horizontal direction [7]. Similarly, the amplitude function is clearly changing most rapidly in the vertical direction. This allows us to consider separable channel filters along the horizontal and vertical directions.

- adaptive bandpass filter design

The filters were implemented using a piecewise-linear approximation in the frequency domain. This guarantees the convergence of filters to the ideal response as the number of filter coefficients goes to infinity [8]. Furthermore, closed-form expressions for the filter coefficients allow us to re-design the filter specifications, and re-compute the filter coefficients online [9]. The amplitude responses of the 11-point coefficient filters that were used are shown in Figure 2.

- fast, single instruction multiple data (SIMD) implementations

Fast implementations are possible using the SIMD extensions of the Pentium III/4 architecture. Fast one-dimensional and two-dimensional FFTs have been developed by the first author [6, 9], allowing speedups in the order of 2-5 times over the fastest, non-SIMD implementations.

- very low effective frame rate in M-mode ultrasound

M-mode ultrasound video tracks a line of pixels through time. The effective frame rate is in the order of about a frame per second. This rate is substantially less than the 30-60 frames per second required for B-mode ultrasound video.

2.2 Robust AM-FM demodulation

A unique challenge associated with the real-time implementation is to provide robust demodulation. Essentially, this problem arises due to the small number of bandpass filters that are used for demodulation. We address the problem in two steps. First, we develop a method for identifying points where the demodulation algorithm may fail. Then, we replace the estimates at these points by smoothed estimates.

To assess the AM-FM demodulation performance at a particular point, we use the instantaneous frequency vector estimate. If the instantaneous frequency vector is outside the main lobes of the magnitude responses of the channel filters, the estimates are assumed to be unreliable (see Figure 2). Naturally, we also require that the instantaneous frequency vectors are not "close" to the first zeros of the magnitude responses. This approach was first proposed in [3].

At pixels where the demodulation estimates are assumed unreliable, we use smoothed estimates. At these pixels, a 5-point, separable, Gaussian window (with $\sigma = 2$) is used for smoothing.

3. RESULTS

Two channel filters were implemented. The first filter was defined to be the tensor product of the right filter with itself (whose magnitude response is) shown in Figure 2, and allowed us to filter both the rows and the columns in the same way. The second filter was defined to be the tensor product of the two filters.

For the video image of Figure 1, the amplitude $a(x,y)$, fundamental FM harmonic $\cos\phi(x,y)$, and fundamental AM-FM harmonic $a(x,y)\cos\phi(x,y)$ estimates are shown in Figure 3. The regions where the demodulation estimates are not found to be reliable are also shown in Figure 3. The AM-FM reconstruction over both filters (with smoothing) is shown in Figure 4(b). Furthermore, as an approximation to the wall boundaries, we consider the FM series (using first filter estimates only, see Figure 4(c))

$$g(x,y) = \sum_{n=1}^{n=20} \cos[n\phi(x,y)].$$

Results from AM-FM segmentation are shown in Figures 4(d) and 4(e). In both cases, we first removed all low-instantaneous frequency magnitude pixels by requiring that $\|\nabla\phi(x,y)\| > 0.1$. Then, we removed all low amplitude pixels by requiring that $a(x,y) > 100$ for Figure 4(d), and $a(x,y) > 38$ for Figure 4(e). Then, both images were filtered using an Alternating Sequential Filter (ASF) at a scale of 5, using a '+' as a structural element (see [10]). The segmentation process helped us identify the septum and left-ventricle walls.

4. CONCLUSION

The initial segmentation results show great promise, but the results will have to be validated over a larger database of M-mode images. Perhaps the most promising result was the ability

of the FM series to track the wall boundaries as shown in Figure 4(c). Ongoing research at the image and video Processing and Communications Lab (ivPCL) is focused on integrating the AM-FM methods to B-mode ultrasound, and then use the results in a 3-D cardiac reconstruction system.

Acknowledgments

The authors would like to thank the Echocardiography Lab in the UNM Children's Heart Center for providing many hours of training and support for this project. This project would not have been possible without their help.

5. REFERENCES

[1] X. Papademetris and J. S. Duncan, "Cardiac Image Analysis: Motion and Deformation," in *Handbook of Medical Imaging: Processing and Analysis,* edited by M. Sonka and J. M. Fitzpartrick, pp. 675-710, SPIE Press, Bellingham, Washington, 2000.

[2] M.S. Pattichis, "AM-FM Transforms with Applications." Ph.D. diss., The University of Texas at Austin, 1998.

[3] J.P. Havlicek, "AM-FM Image Models." Ph.D. diss., The University of Texas at Austin, 1996.

[4] M. S. Pattichis, G. Panayi, A. C. Bovik, and H. Shun-Pin, "Fingerprint Classification Using an AM-FM Model," *IEEE Transactions on Image Processing,* vol. 10, no. 6, pp. 951-954. June 2001.

[5] M.S. Pattichis and A.C. Bovik, "Multi-Dimensional Frequency Modulation in Texture Images," in *Proc. International Conference on Digital Signal Processing*, Limassol, Cyprus, June 26-28 1995, pp. 753-758.

[6] P. Rodríguez V, "A Radix-2 and FFT Algorithm for Modern Single Instruction Multiple Data (SIMD) Architectures, " submitted to *Signal Processing Letters.*

[7] P. Rodriguez V. and M.S. Pattichis, "Adaptive Sampling and Processing of Ultrasound Images," 5 pages, published in Proc. *35th Asilomar Conference on Signals, Systems, and Computers*, Asilomar Hotel and Conference Grounds, Pacific Grove, CA, November, 2001.

[8] M.S. Pattichis, ``Least Squares FIR Filter Design Using Frequency Domain Piecewise Polynomial approximations," published in the proceedings of *Xth European Signal Processing Conference*, Tampere, Finland, September 5-8, 2000.

[9] .P. V. Rodriguez, M. S. Pattichis, and R. Jordan, "Computational SIMD Framework: split-radix simd-fft algorithm, derivation, implementation and performance," in Proc. of *14th International Conference on DSP (DSP 2002)*, Santorini, Greece, July 2002.

[10] E.R.Dougherty, *An Introduction to Morphological Image Processing,* Belingham, Washington, SPIE Optical Engineering Press, 1992.

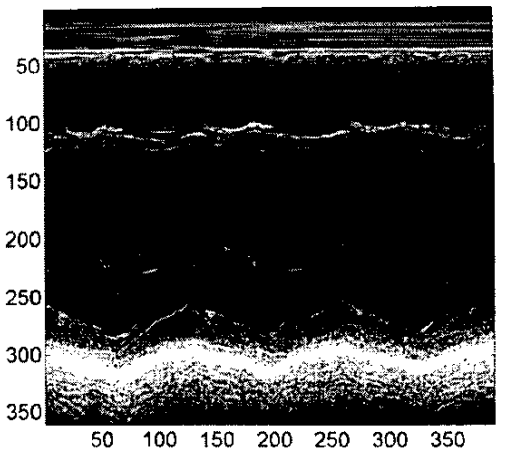

Figure 1. An M-mode ultrasound video image.

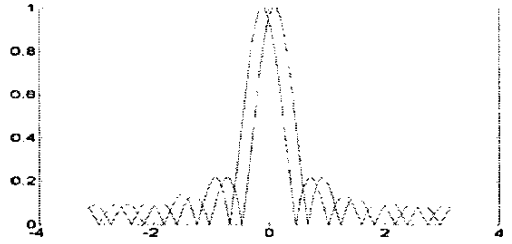

Figure 2. Magnitude response of the two 11-coefficient digital filters. It is important to note that the zeros of each filter approximately correspond to near-maxima of the other.

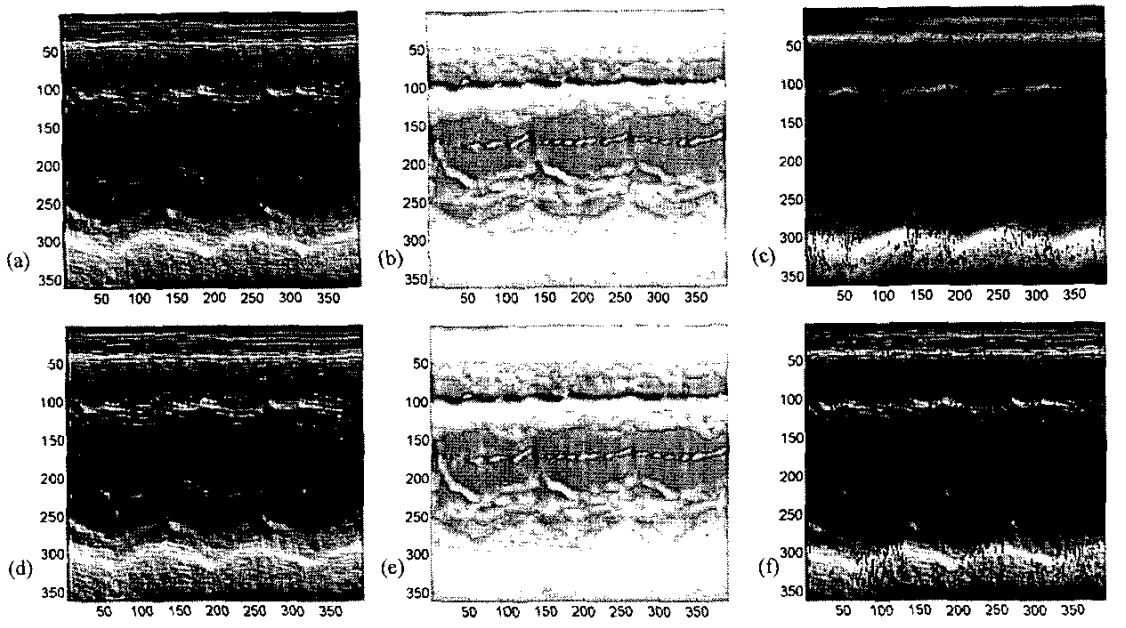

Figure 3. AM-FM estimates over both channel filters. The amplitude estimates $\hat{a}(x,y)$ are shown in 3(a) and 3(d). The FM estimates $\cos\hat{\phi}(x,y)$ are shown in 3(b) and 3(e). The AM-FM estimates $\hat{a}(x,y)\cos\hat{\phi}(x,y)$ are shown in 3(e) and 3(f). In 3(e) and 3(f), we note that image regions where demodulation estimates are "unreliable" are shown in black, often appearing as vertical lines through the image.

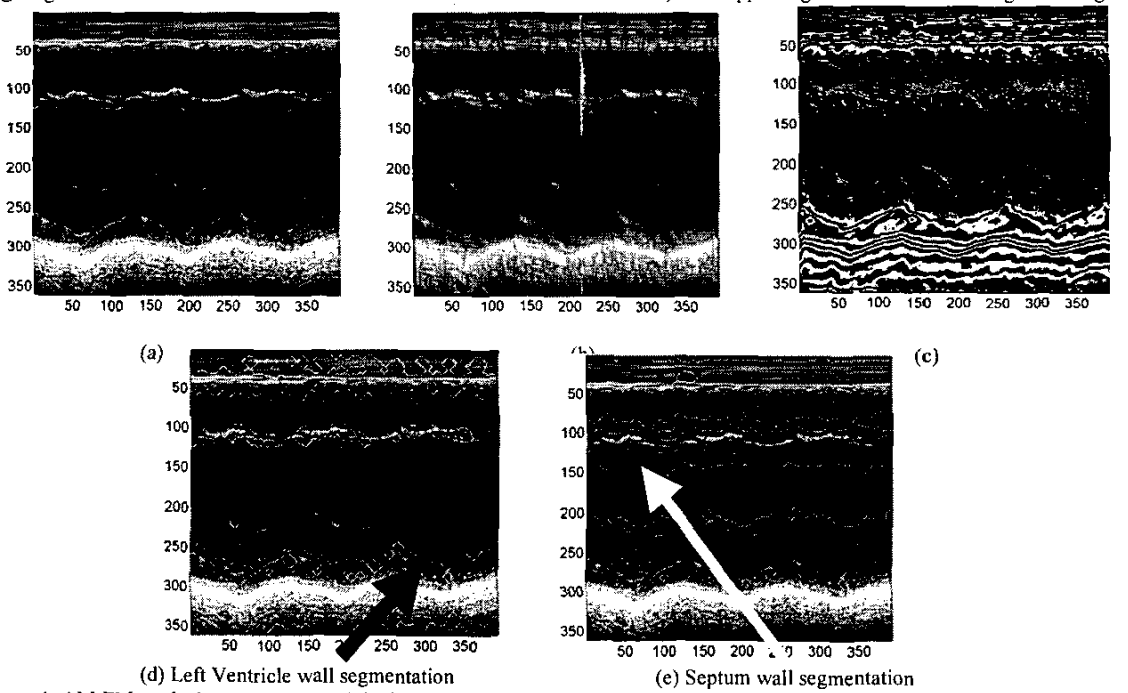

(d) Left Ventricle wall segmentation (e) Septum wall segmentation

Figure 4. AM-FM analysis results. The original image is shown in 4(a). In 4(b), the AM-FM reconstruction over both channel filters (with smoothing) is shown. In 4(c), the FM series sum is shown. In 4(d) and 4(e), we show results of AM-FM segmentation. In 4(c), low-amplitude pixels $a(x,y) \leq 100$ are set to zero, and the resulting image is binarized by thresholding in the intersection of the resulting bimodal distribution (not shown).